J Eng Math (2010) 68:197–205
DOI 10.1007/s10665-010-9371-2

Stability of hydraulic fall and sub-critical cnoidal waves in water flows over a bump

A. S. Donahue · S. S. P. Shen

Received: 15 June 2009 / Accepted: 5 April 2010 / Published online: 21 April 2010

Abstract A forced Korteweg–de Vries (fKdV) equation can be used to model the surface wave of a two-dimensional water flow over a bump when the upstream Froude number is near one. The fKdV model typically has four types of solutions: sub-critical cnoidal waves, sub-critical hydraulic fall, transcritical upstream soliton radiation, and supercritical multiple solitary waves. This paper provides a numerical demonstration of the stability of the hydraulic falls and cnoidal waves solutions.

Keywords Cnoidal waves · Forced Korteweg–de Vries equation · Hydraulic fall · Stability · Stability of hydraulic fall and cnoidal waves · Water waves

1 Introduction

This paper studies the stability of two-dimensional surface waves of an upstream uniform water flow over a bump (see Fig. 1 for the physical model and see [1, Chap. 2] for various applications and theoretical studies of the model). Our current study is limited to a model of a moderate size bump so that the forced Korteweg–de Vries (fKdV) equation can be used as the model equation [2–5]. Our objective is to demonstrate the stability of sub-critical steady-state surface profiles, which are either a hydraulic fall or a cnoidal wave.

The fKdV equation has been found as an appropriate model for the water motion forced by a moving bump under the assumptions that the upstream Froude number is near one, the bump's base is relatively short compared to the length of the surface waves, and the bump height is relatively small compared to the wave amplitude [4], [6–9]. The fKdV equation can be derived from a formal perturbation analysis by introducing a small parameter ϵ [6, 7, 10]. Although no mathematical proof has been given, several studies concluded that the fKdV is an accurate equation to model the said flow [4, 8]. Typically, the fKdV has four types of solutions: steady-state sub-critical cnoidal waves [1, pp. 59–61], [11] steady-state hydraulic fall [12], unsteady transcritical upstream soliton radiation [7, 8, 13, 14], and steady-state supercritical multiple solitary waves [9, 15]. For multiple supercritical solitary waves, Malomed [16] proved that the higher solitary wave is unstable. Camassa and Wu [17] showed that certain lower solitary waves

A. S. Donahue · S. S. P. Shen (✉)
Department of Mathematics and Statistics, San Diego State University, San Diego, CA 92182, USA
e-mail: shen@math.sdsu.edu

A. S. Donahue
e-mail: adonahue@rohan.sdsu.edu

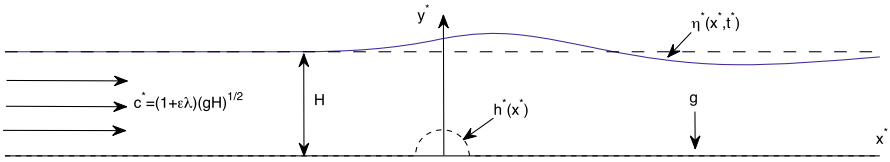

Fig. 1 A schematic model for a water flow in a channel with a bump at the bottom: x^* and y^* are the horizontal and vertical spatial axes, H is the depth of the channel, g is the gravitational constant, $h^*(x^*)$ represents the shape profile of the local bump, $\eta^*(x^*, t^*)$ represents the vertical displacement of the water surface, and c^* is the upstream near-critical flow speed which has a Froude number close to 1

are stable. Shen et al. [5] numerically demonstrated that the upper solitary wave is unstable and the lower one is stable. The stability of the sub-critical steady-state waves, including the hydraulic fall and cnoidal waves, has not yet been numerically demonstrated or mathematically proven. These steady-state surface profiles are included in the generalised critical free-surface flows over a bump proposed by Dias and Vanden-Broeck [2].

Forbes observed the hydraulic fall in a laboratory [12], and he and others also numerically found hydraulic falls by solving the boundary-value problem of the fully nonlinear Euler equations [12, 15, 18, 19]. Forbes and Schwartz also identified applications of the hydraulic fall solutions in atmospheric flows [18]. The hydraulic fall was a special case of a sub-critical cnoidal wave when the sub-critical Froude number was equal to a specific value. The current paper will demonstrate that both the cnoidal wave and the hydraulic fall as solutions of the fKdV model are stable.

The text of this paper is arranged as follows. Section 2 recapitulates the cnoidal wave and hydraulic fall solutions of the fKdV equation, and describes the numerical method used. Section 3 describes stability simulation results. Conclusions are given in Sect. 4.

2 Method

The physical model of our uniform water flow over a bump is in a two-dimensional channel as shown in Fig. 1. The upstream water depth of the channel is given as H. The variable $y^* = H + \eta^*(x^*, t^*)$ represents the height of the water surface at position x^* and time t^*. The bottom topography of the channel is described by $y^* = h^*(x^*)$ and has a compact support. The upstream velocity $c^* = (1 + \epsilon\lambda)\sqrt{gH}$ has a Froude number near one 1.0, where g is the gravitational acceleration, ϵ is a small perturbation parameter related to the ratio between the water depth H and the typical wave length L, and λ is a control parameter that measures the perturbation of the upstream flow velocity away from the critical speed. The following dimensionless variables are introduced for the variables in the fKdV model:

$$\epsilon = \left(\frac{H}{L}\right)^2 \ll 1 \quad c = \frac{c^*}{\sqrt{gH}}$$

$$x = \frac{x^*}{L} \quad y = \frac{y^*}{H}$$

$$t = \epsilon^{3/2}\sqrt{\frac{g}{H}}t^* \quad \eta = \frac{\eta^*}{\epsilon H}$$

When ignoring the second-order term $O(\epsilon^2)$, the water-surface profile function is approximately governed by a fKdV partial differential equation. When the bottom bump's base is relatively short compared to the wave length, the forcing term in the fKV model may be approximated by a Dirac delta function. The mathematical model of our water flow problem over a bump is then described by the following initial-value problem (IVP) of the fKdV:

$$\eta_t + \lambda\eta_x - \frac{3}{2}\eta\eta_x - \frac{1}{6}\eta_{xxx} = \frac{P}{2}\delta_x(x), \tag{1a}$$

$$\eta(x, t = 0) = f_0(x), \tag{1b}$$

$$\eta^{(n)}(x = \pm\infty, t) = 0 \quad \text{for } n = 0, 1, 2. \tag{1c}$$

Here, the forcing term $\frac{P}{2}\delta_x(x)$ is determined by the bump's size, $\delta(x)$ is the Dirac delta function, $\delta_x(x)$ stands for the derivative of $\delta(x)$, η_t and η_x are partial derivatives with respect to t and x, respectively, and $f_0(x)$ is the initial profile of $\eta(x,t)$ [10, pp. 168–171]. The surface-wave profile of the water in the channel is given by $y(x,t)H = [1+\epsilon\eta(x,t)]H$.

2.1 Hydraulic fall and cnoidal wave solutions to the fKdV equation

Stationary sub-critical stationary solutions $v(x)$ to the fKdV, Eq. 1, are being considered when the Froude number is near one but less than 1.0, hence $\lambda < 0$. We substitute $v(x) = \eta(x,t)$ a steady state solution in Eq. 1 to represent the time independence of the stationary solutions. Thus, stationary sub-critical solutions to the fKdV can be found by solving the following second-order ordinary differential equation (ODE) with the given upstream conditions.

$$\lambda v - \frac{3}{4}v^2 - \frac{1}{6}v'' = \frac{P}{2}\delta(x) \tag{2a}$$

$$v(-\infty) = v'(-\infty) = 0 \tag{2b}$$

It can be shown that there exists a critical value

$$\lambda_L = \left(\frac{-81P^2}{32}\right)^{\frac{1}{3}} < 0 \tag{3}$$

such that the above ODE under the given conditions (2) has (i) a cnoidal-wave solution for $\lambda < \lambda_L$, (ii) a hydraulic fall solution when $\lambda = \lambda_L$, and (iii) no bounded solutions when $0 > \lambda > \lambda_L$ [10, p. 159].

2.1.1 Cnoidal-wave solution

In the case of $\lambda < \lambda_L$, the problem (2) has a cnoidal wave solution which can be expressed in terms of a Jacobi elliptic function

$$v(x) = \frac{-4\lambda}{3}\left[-\cos\left(\theta+\frac{4\pi}{3}\right) - \frac{1}{2} + \left(\cos\left(\theta+\frac{4\pi}{3}\right) - \cos\left(\theta+\frac{2\pi}{3}\right)\right) \times \mathrm{cn}^2\left(\sqrt{-\lambda\left(\cos\theta - \cos\left(\theta+\frac{2\pi}{3}\right)\right)}(x-x_0), k^2\right)\right] \tag{4}$$

for $x > 0$. The phase shift x_0 is determined by the initial value $v(0+) = 0$. The parameters k^2 and θ are given as follows:

$$\theta = \frac{1}{3}\arccos\left(1 + \frac{81P^2}{16\lambda^3}\right), \tag{5}$$

$$k^2 = \frac{\cos\left(\theta+\frac{4\pi}{3}\right) - \cos\left(\theta+\frac{2\pi}{3}\right)}{\cos(\theta) - \cos\left(\theta+\frac{2\pi}{3}\right)}. \tag{6}$$

Thus, the free-surface profile is zero upstream and is a cnoidal wave downstream. Note that as λ approaches λ_L, k^2 approaches 1 and the solution becomes a hydraulic fall.

2.1.2 Hydraulic-fall solution

Letting $\lambda = \lambda_L$ we can simplify Eq. 4 to get the solution

$$v(x) = \frac{-4\lambda_L}{3}\left[-1 + \frac{3}{2}\mathrm{sech}^2\left(\sqrt{\frac{-3\lambda_L}{2}}(x-x_0)\right)\right], \tag{7}$$

where x_0 is determined by $v(0+) = 0$, i.e.,

$$x_0 = \sqrt{\frac{-2}{3\lambda_L}}\operatorname{arcsech}\sqrt{\frac{2}{3}}. \tag{8}$$

The free-surface profile falls from zero upstream to $4\lambda_L/3 < 0$ downstream. This is the hydraulic fall.

2.2 Numerical method for the stability simulation

The stability simulation is to solve an initial-value problem (IVP) for the time-dependent fKdV equation (see Eq. 1). The initial condition of the IVP is either the sub-critical stationary solution or the sum of the sub-critical stationary solution with a white noise as an explicit perturbation. The semi-implicit spectral method is used to solve the IVP. This approach is the same method used to simulate the stability of the supercritical lower solitary waves and the instability of the supercritical upper solitary waves [5]. The semi-implicit algorithm means that the linear algebraic equations can be solved by a simple analytic method rather than the numerical methods for solving the full simultaneous linear algebraic equation. The scheme is stable for a wide range of spatial resolution and time steps, and the algorithm is very fast.

The stationary solution is perturbed by the numerical integration error of the time-dependent fKdV and an explicit white noise. Because of the use of the spectral method, the error due to the spatial integration has very large wave numbers. Because of the small time step, the error due to the time gap has very high frequencies. Another error in our spectral method is boundary reflection of the fast-propagating waves of high frequency in time and high wave-number space. The numerical integration errors are considered perturbations to the stationary solutions. To further demonstrate the solutions stability, we also explicitly added a white noise to the stationary solutions. The sum of the stationary solutions and the white noise is used as the initial condition of the time-dependent fKdV equation. Therefore, the original sub-critical cnoidal waves and the hydraulic fall were perturbed by the numerical truncation error and the white noise forcing. As the time elapses, the white noise dissipates and the solution converges to the sub-critical stationary solutions: cnoidal waves or a hydraulic fall. For the same initial condition, the numerical simulations were repeated for many different realizations of white noise, and the same decay of the white noise was observed. We have also performed simulations for different control parameters of the flow model: P and λ. Altogether we have made stability simulations for 64 pairs of control parameters for $-0.5789 \le P \le 0.5789$ and $1.5\lambda_L \le \lambda \le \lambda_L$. Again, similar numerical results about stability have been observed for all the cases. The results of four cases are presented in the next section.

Of course, if the original stationary solution were unstable, the solution of the IVP would not converge to the stationary solution. For example, the unstable supercritical upper solitary wave converges to the lower solitary wave (which is stable) and radiates a free soliton away [5].

We thus numerically integrate the initial value problem of the fKdV equation (1) in a given interval $-W < x < W$ with the initial condition $\eta(x, t = 0) = v(x) + w(x)$, where $w(x)$ is the spatial white noise. The finite spatial interval requires appropriate boundary conditions at both end points $x = \pm W$. When simulating the stability of solitary waves, the end conditions at $x = \pm W$ are zero and hence satisfy the periodicity required by the spectral method used. When simulating the stability for cnoidal waves and hydraulic falls, the boundary conditions at $x = W$ are no longer zero, and a difficulty arises. If we regard the physics model as the surfaces generated by a moving bump at the bottom of a rest water, then the disturbance should be zero at $\pm\infty$. Thus the cnoidal waves and hydraulic falls can be regarded as the phenomena observed near the bump (see the boundary condition (1c)). Motivated by this idea, we overcome the above difficulty by using a very large W and letting the stationary solution extend only to $\pm(1/2)W$. Hence the end conditions at $x = \pm W$ are still zero. The discontinuity at $x = (1/2)W$ triggers a disturbance wave that propagates both upstream and downstream; see Fig. 2. In the numerical simulation, W is chosen to be sufficiently large so that the solution local to the forcing is not affected by this disturbance wave over the course of our stability simulation. The speed and stability of the scheme allows for the use of rather large W values and small time steps to ensure a good accuracy. In all of the numerical simulations discussed in this paper we

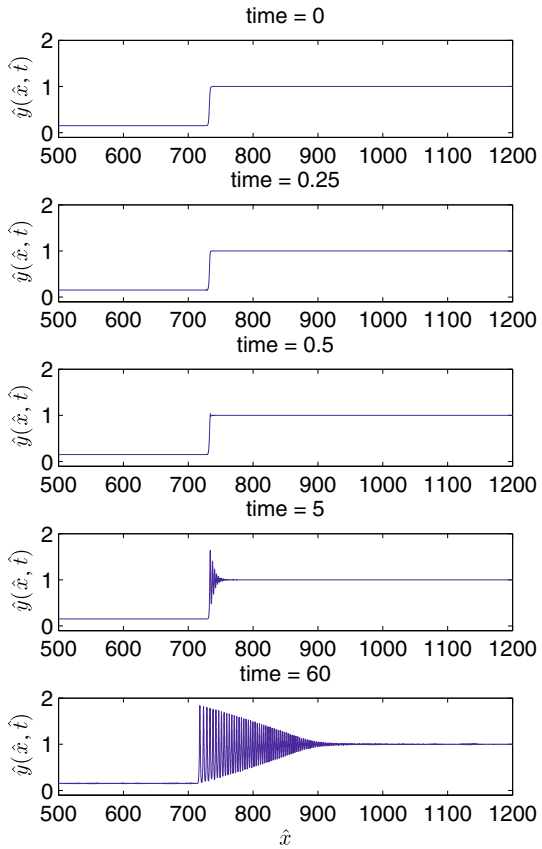

Fig. 2 The time evolution of the disturbance wave caused by the discontinuity at $\hat{x} = 732$

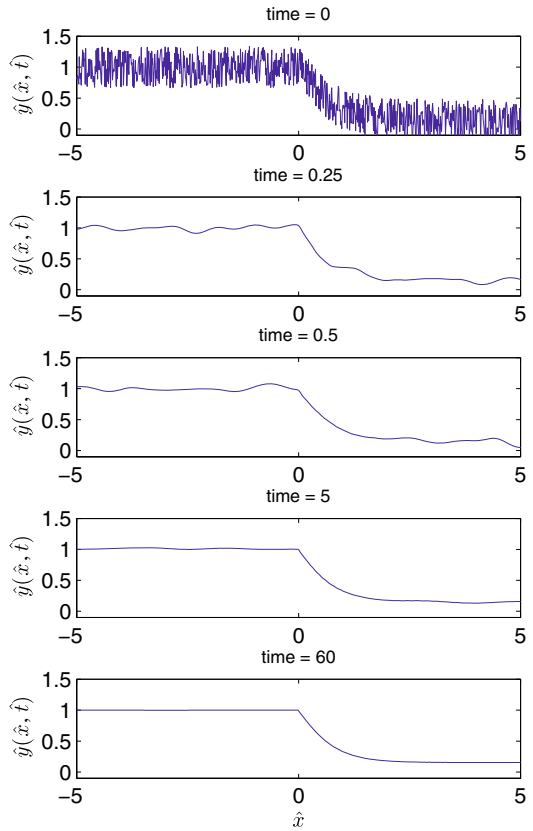

Fig. 3 The time evolution of a white-noise-perturbed hydraulic fall solution to the fKdV equation with a positive bump forcing: $\hat{y} = 1 + \epsilon\eta(\hat{x},\hat{t})$. Both the vertical and horizontal length scales are $H = 66.67$ mm. The time scale is $T = \epsilon^{-1/2}\sqrt{H/g} = 0.08$ s. Thus $\hat{y}H$, $\hat{x}H$ and $\hat{t}T$ are the laboratory space and time scales

take $W = 1200$ with a time step of $\Delta t = 0.005$ and the total number of points in the x-axis is 2^{18}, which implies a spatial step $\Delta x = 0.0092$.

When observing the stability of the cnoidal waves and hydraulic fall, we only need to explore the perturbation decay and the shape maintenance in the vicinity of the bump with $x^* = xL$ in both the downstream and upstream directions by at most 4 or 5 H. Figure 2 indeed shows that the disturbance waves are far away from the vicinity of the bump during the entire course of our stability simulation.

3 Results

The results of stability simulations for four cases are presented here: hydraulic fall with a positive bump, cnoidal waves with a positive bump, a humped hydraulic fall with a negative bump (i.e., a dent), and humped cnoidal waves with a negative bump.

Figures 3–6 show the stability of the four cases with $P = 0.5789$. The value P is given by the relationship between the upstream water depth and the radius of the bump, $P = \frac{\pi}{2}(\frac{R}{H})^{5/4}$. Here H is the upstream depth of the water and is the vertical scale of the water body, and R is the radius of the semi-circular bump. Since the

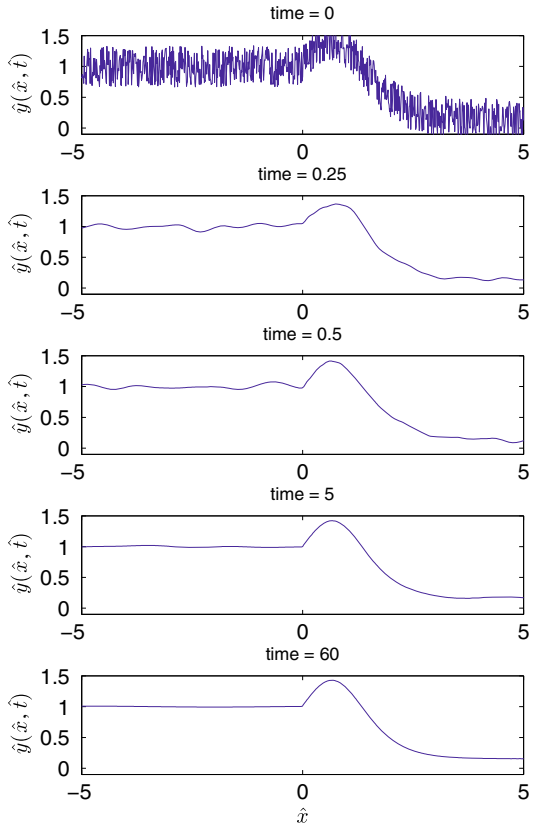

Fig. 4 The time evolution of a white-noise-perturbed hydraulic fall solution to the fKdV equation with a dent forcing. The scales are the same as in Fig. 3

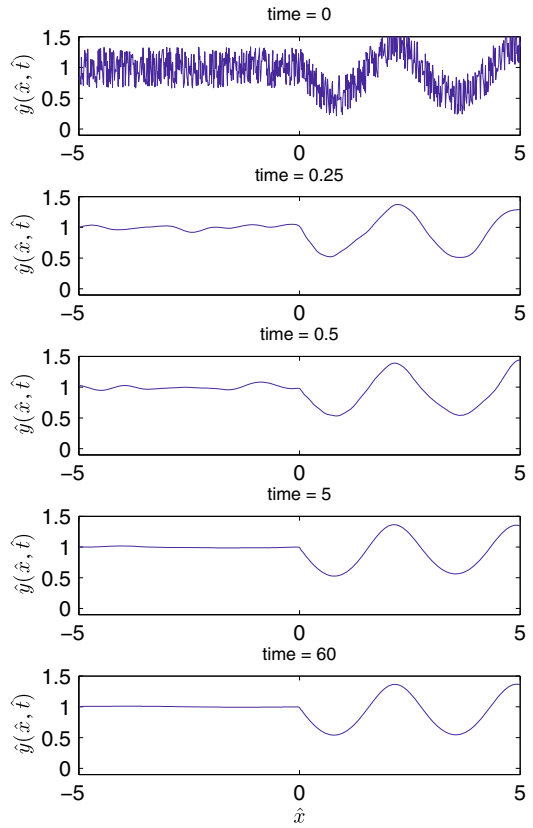

Fig. 5 The time evolution of a white-noise-perturbed cnoidal wave solution to the fKdV equation with a positive bump forcing. The scales are the same as in Fig. 3

fKdV equation is an asymptotic mathematical model, it involves a small dimensionless quantity $\epsilon = \sqrt{R/H}$. This small quantity is not uniquely defined according to the ϵ-invariant theorem [9]. In all the solutions given in this paper $\epsilon = 0.67$. The horizontal scale is given as $L = H/\epsilon^{1/2}$. The time scale is $T = L/\sqrt{gH}$, where g is the gravitational acceleration. In the laboratory, Forbes [20] tested a system with $R = 30\,\text{mm}$ and $H = 66.67\,\text{mm}$. This gives us a horizontal scale of $L = 81.4\,\text{mm}$ and a time scale of $T = 0.10\,\text{s}$. With these scaling factors the asymptotic analysis uses the following dimensionless quantities in (1) and (2); $x = \frac{x^*}{L}$, $y = \frac{y^*}{H}$ and $t = \frac{t^*}{T}$ [10, p. 149].

3.1 Case 1: Hydraulic fall with positive bump

The variables x, y and t in (2) are the dimensionless variables resulted from the asymptotic analysis [10, p. 149]. In order to match the laboratory observation and provide comparison to the experiments conducted by Forbes [20], a rescaling is made. We transform the variables x, y and t into the following dimensionless quantities, $\hat{x} = \epsilon^{-1/2}x$, $\hat{y} = y$ and $\hat{t} = \epsilon^{-1/2}t$. This removes the constant L from the non-dimensionalization procedure of the system, making the length scaled only by $H = 66.67\,\text{mm}$ and the time scaled by $\sqrt{H/g} = 0.08\,\text{s}$.

Figure 3 shows the stability of a hydraulic fall with a positive bump. When $\hat{t} = 0$, the hydraulic fall is perturbed by a uniformly distributed white noise found by calculating a random value between -0.5 and 0.5 at each value of x and adding it to the stationary solution. It can be seen in the figure that the noise dissipates very quickly. When $\hat{t} = 0.25$, the high-wave-number part of the noise has dissipated, and only some slow oscillations remain

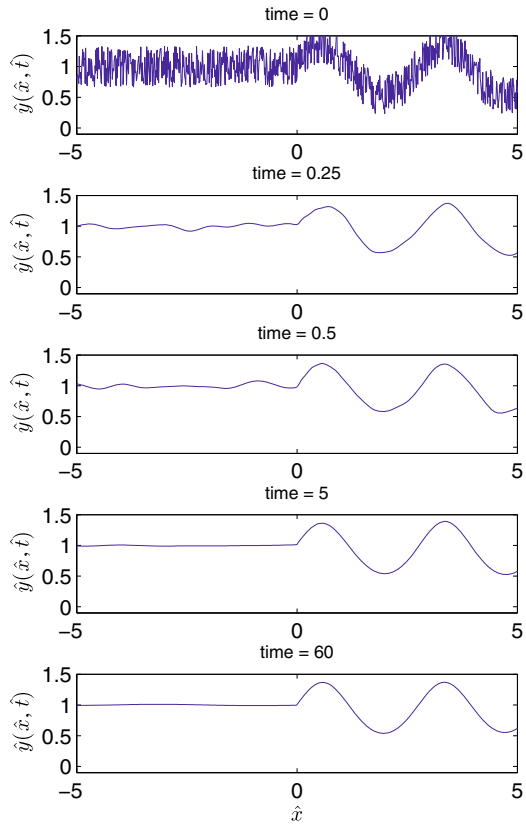

Fig. 6 The time evolution of a white-noise-perturbed cnoidal wave solution to the fKdV equation with a dent forcing. The scales are the same as in Fig. 3

in the surface profile. When $\hat{t} = 0.5$, much of the slow oscillations have disappeared. When $\hat{t} = 5$, the perturbed hydraulic fall has nearly restored into the pure hydraulic fall. At $\hat{t} = 10$, the hydraulic fall is completely restored. Further simulation into $\hat{t} = 60$, corresponding to a lab time 4.9 s, still demonstrates the same stable hydraulic fall.

This case has the same parameters as an experiment conducted by Forbes [12] for the case of a positive semi-circular bump of radius $R = 30$ mm and water depth $0.45H = R$. In this experiment, Forbes found that the ratio between the depth of the channel upstream of the bump to the depth of the channel downstream of the bump was 0.2. Our numerical results found that ratio to be 0.15.

The sharp corner of the water-surface profile is an artifact due to the Dirac delta approximation to the bump in the fKdV model in the case of a short bump [3]. Forbes' actual laboratory observation does not have this sharp corner at the site of the bump [12].

3.2 Case 2: Hydraulic fall with negative bump

The negative bump means a dent forcing [11]. With the negative bump, the water surface has a hump immediately downstream of the dent. The hump smoothly falls into a lower level of flat surface. The lower horizontal surface is at the same height as the positive bump of the same size as shown in Fig. 3.

Figure 4 shows the stability of this kind of hydraulic fall. The hydraulic fall is perturbed by a uniformly distributed white noise at the initial time $\hat{t} = 0$. The perturbed hydraulic fall is used as the initial condition of the time dependent fKdV equation. The white noise dissipates away very quickly as in the case of a positive bump.

3.3 Case 3: Cnoidal wave with positive bump

Figure 5 shows the stability of a cnoidal wave with a positive bump. At the initial time $\hat{t} = 0$ the wave is perturbed by a uniformly distributed white noise of random values chosen from a range between -0.5 and 0.5. Again, the noise dissipates very quickly, and by $\hat{t} = 5$ the noise is nearly all gone. Further simulation into $\hat{t} = 60$ shows that the cnoidal wave has been well maintained.

3.4 Case 4: Cnoidal wave with negative bump

Figure 6 shows the effect of a dent forcing on the cnoidal wave solution. The free surface also has a hump immediately downstream of the bump. This is the same as the dent forcing for the hydraulic fall. The dent-forced cnoidal wave solution is initially perturbed by a uniformly distributed white noise as in Case 3. In very little time the perturbation has dissipated, leaving behind a smooth cnoidal wave solution. By time $\hat{t} = 5$ the noise has almost entirely dissipated. Further simulation into time $\hat{t} = 60$ demonstrates the stability of the cnoidal-wave solution.

4 Conclusions and discussion

We have numerically demonstrated the stability of the two forms of sub-critical stationary solutions to the fKdV equation: cnoidal waves and a hydraulic fall. The spectral method was employed in our numerical scheme and parameter values were chosen to match an experiment conducted by Forbes [12]. We have shown that both the solutions are stable. Each type of solution was tested for two cases of forcings, once with a positive forcing bump and again with a negative dent forcing. In all four cases, the initial condition was perturbed by white noise and integrated over time. In each case the same dynamics were observed: in a short time most of the white noise had dissipated, and by time $t^* = 0.4\,\mathrm{s}$, all the white-noise-perturbed surface profiles have been almost completely restored to their original shapes. Further integration up to the time $t^* = 4.9\,\mathrm{s}$ still shows the stable initial profile, and hence has demonstrated the stationary solution's stability. We have also demonstrated the stability for different values of the control parameters λ and P, and altogether 64 cases have been simulated.

Our numerical method can thus effectively overcome the difficulty of non-zero downstream boundary conditions. However, the efficiency of this scheme is not known. We have no theory to choose a minimum W a priori to make the numerical method the most efficient. In addition, it is worth investigating whether appropriate boundary conditions can be derived so that the stability simulation can be made only in the physical interval of interest, i.e., $-5H < x^* < 5H$.

Introducing the length of the downstream waves as a third control parameter in the model of Fig. 1, Dias and Vanden-Broeck [2] identified three other solutions in their bifurcation diagram besides the four typical solutions listed in our introduction. These three solutions are a solitary wave in the transcritical regime, a reversed hydraulic fall [11], and reversed downstream cnoidal waves. The stability of the reversed hydraulic fall and the reversed downstream cnoidal waves is still to be demonstrated.

Recently, Binder and his collaborators considered various kinds of bumps, including two bumps, a step, a bump and a dent, and others [21–27]. Various kinds of surface-wave profiles were found. Again, the stability of these steady-state surface profiles is still to be demonstrated.

Further work still needs to be done in mathematically proving that the cnoidal wave and hydraulic fall solutions are stable. The works of Malomed [16] and Camassa and Wu [17] seem to indicate that the proof can be mathematically challenging even for the case of linear stability, because the associated eigenvalue problem is for a non-self-adjoint differential operator and the determination of the signs of the real part of the eigenvalue hence appears difficult. To our knowledge, a rigorous analytical proof of the stability or instability of all the known stationary profiles of the fKdV model is yet to be provided.

Acknowledgments This research is partially supported by a Canadian NSERC grant and a San Diego State University's UGP grant.

References

1. Baines PG (1995) Topographic effects in stratified flows. Cambridge University Press, Cambridge
2. Dias F, Vanden-Broeck JM (2002) Generalised critical free-surface flows. J Eng Math 42:291–301
3. Miles J (1986) Stationary, transcritical channel flow. J Fluid Mech 162:489–499
4. Shen SSP (1995) On the accuracy of the stationary forced Korteweg-de Vries equation as a model equation for flows over a bump. Q Appl Math 53(4):701–719
5. Shen SSP, Manohar R, Gong L (1995) Stability of the lower cusped solitary waves. Phys Fluid 7:2507–2509
6. Akylas T (1984) On the excitation of long nonlinear water waves by a moving pressure distribution. J Fluid Mech 141:455–466
7. Grimshaw RHJ, Smyth NF (1986) Resonant flow of a stratified fluid over a topography. J Fluid Mech 169:429–464
8. Lee S, Yates G, Wu TY (1989) Experiments and analyses of upstream-advancing solitary waves generated by moving disturbances. J Fluid Mech 199:569–593
9. Shen SSP (1992) Forced solitary waves and hydraulic falls in two-layer flows. J Fluid Mech 234:583–612
10. Shen SSP (1993) A course on nonlinear waves. Kluwer, Boston
11. Shen SSP (1991) Locally forced critical surface waves in channels of arbitrary cross section. J Appl Math Phys (ZAMP) 42(1): 122–138
12. Forbes L (1988) Critical free-surface flow over a semi-circular obstruction. J Eng Math 22:3–13
13. Smyth NF (1987) Modulation theory solution for resonant flow over topography. Proc R Soc Lond A 409:79–97
14. Wu TY (1987) Generation of upstream advancing solitons by moving disturbances. J Fluid Mech 184:75–99
15. Vanden-Broeck JM (1987) Free-surface flow over an obstruction in a channel. Phys Fluid 30:2315–2317
16. Malomed B (1988) Interaction of a moving dipole with a soliton in the KdV equation. Phys D 32(3):393–408
17. Camassa R, Wu TY (1991) Stability of forced steady solitary waves. Philos Trans R Soc Lond A 337:429–466
18. Forbes L, Schwartz L (1982) Free-surface flow over a semicircular obstruction. J Fluid Mech 114:299–314
19. Zhang D, Chwang A (1999) On solitary waves forced by underwater moving objects. J Fluid Mech 389:119–135
20. Forbes L (1989) Two-layer critical flow over a semi-circular obstruction. J Eng Math 23:325–342
21. Binder BJ, Dias F, Vanden-Broeck JM (2005) Forced solitary waves and fronts past submerged obstacles. Chaos 15:037106-1–037106-13
22. Binder BJ, Dias F, Vanden-Broeck JM (2006) Steady free-surface flow past an uneven channel bottom. Theor Comput Fluid Dyn 20:125–144
23. Binder BJ, Dias F, Vanden-Broeck JM (2007) Influence of rapid changes in a channel bottom on free-surface flows. J Appl Math 73:254–273
24. Dias F, Vanden-Broeck JM (2004) Trapped waves between submerged obstacles. J Fluid Mech 509:93–102
25. Gong L, Shen SSP (1994) Multiple supercritical solitary wave solutions of the stationary forced Korteweg-de Vries equation and their stability. SIAM J Appl Math 54:1268–1290
26. Grimshaw RHJ, Zhang DH, Chow KW (2007) Generation of solitary waves by transcritical flow over a step. J Fluid Mech 587:235–254
27. Shen SSP, Gong L (1992) Solitary waves on a shelf. Phys Fluid A 5:1071–1073